Desalination and Water Treatment
www.deswater.com
1944-3994/1944-3986 © 2013 Desalination Publications. All rights reserved
doi: 10.1080/19443994.2012.707374

51 (2013) 1503–1510
February

Taylor & Francis
Taylor & Francis Group

Numerical simulation of forced convective evaporation in thermal desalination units with vertical tubes

R. Kouhikamali*, B. Hassanpour, K. Javaherdeh

Faculty of Engineering, University of Guilan, Rasht, Iran
Tel. +98 131 6690276; Fax: +98 131 6690273; email: kouhikamali@guilan.ac.ir

Received 16 March 2012; Accepted 25 June 2012

ABSTRACT

The subject of present study is a numerical simulation of transient solution of evaporation on upward flow in a two-dimensional vertical tubes by using the water as the working fluid. The heat transfer mechanisms are energy and mass transfer during the phase change based on volume of fluid model in commercial CFD software, with a user defined function. Operating conditions are specified in saturation temperature of water flow boiling. The physical properties of water are determined using inlet temperature and pressure system in saturation conditions. The characteristic of water flow boiling such as void fraction, heat transfer coefficient, and wall temperature distribution are investigated in the range of various heat fluxes. Due to agitation of vapor bubbles, the flow is turbulent which is simulated based on SST K–ω model and also the pressure implicit with splitting of operators pressure–velocity coupling scheme is used to improve the efficiency of calculation.

Keywords: Numerical simulation; Forced convective evaporation; VOF method; Vertical tubes

1. Introduction

The heat transfer phenomenon associated with liquid–vapor phase change play an important role in vertical heated tubes of evaporators for the heat exchangers in industries. The configuration for heat exchangers in steam transformers of multiple effect desalination systems, are special interest, where water experiences heat transfer at different levels of pressure. Over the last decade, extensive experimental and theoretical research efforts have been devoted to understanding the fundamental aspects of subcooled and saturated two-phase flow boiling [1].

Steiner and Taborek [2] summarized the various available correlations of saturated flow boiling. Thome [3] studied pool boiling and flow boiling and addressed several key points on flow boiling. Kandlikar [4] performed a historical review on flow boiling heat transfer concepts. McAdams et al. [5] and Prodanovic [6] presented reliable formula for flow boiling regions.

In this article, the evaporation process in evaporator tubes is investigated. The water flow in the evaporator working under forced convection is vertically upward. When the heat flux from the heated wall to the fluid increases above a certain value, the raised up surface temperature superheats the water in contact with the surface. The associated flow boiling is initiated in a certain length called onset of nucleate boiling (ONB). During the flow boiling, the heat transfer is transported from the heated surface to the liquid by

*Corresponding author.

Presented at the International Conference on Desalination for the Environment, Clean Water and Energy, European Desalination Society, 23–26 April 2012, Barcelona, Spain

the latent heat of evaporation [7]. The main purpose of the present study is to simulate the subcooled and saturated flow boiling, when the water flows upward inside the tube which is evaporated by means of a high pressure motive steam outside the tube.

Water enters under its subcooled condition as compressed liquid. There are three important regions inside an evaporation tube: single-phase liquid (pure liquid), subcooled flow boiling, and saturated two-phase flow boiling regions. In subcooled flow boiling region, the bulk liquid temperature must remain below saturation condition.

2. Geometrical configurations

The computation domain and boundaries of a two-dimensional circular tube is illustrated in Fig. 1. The solution domain of two-dimensional circular tube is $X \times Y = 500 \times 38.1$ mm. The inlet and outlet boundary conditions are considered mass flow inlet and pressure outlet, respectively, and the direction of the flow is upward. The heated wall boundary condition is provided as constant temperature. The computational nonuniform grid of domain is 7,050 regular quadrilateral cells. A time step of $\Delta t = 10^{-5}$ s is used to solve this problem.

3. Numerical models

In this paper, the simulation of two-phase flow is carried out by employing volume of fluid (VOF) model in commercial CFD software Fluent 6.3, with a user-defined function. The flow is considered as turbulent based on the Reynolds number. In this simulation, the SST K–ω model is adopted. The low-Reynolds form of the SST K–ω used for turbulence modeling displays a gradual change from the standard K–ω model in the inner region of the boundary layer to a high-Reynolds version of the K–ω model in the outer part of the boundary layer. Also, compared to the standard K–ω model, a modified formulation of the turbulent viscosity is adopted in order to take the transport effects of the principal turbulent shear stress into account. The Green-Gauss node-based method is used for evaluation of gradients. In the laminar sublayer region, the velocity profile is specified linear by means of enhanced wall treatment adjacent the wall. The velocity profile of the buffer region is described by the logarithmic wall function. An implicit time discretization along with the modified High Resolution Interface Capturing (HRIC) scheme is used for VOF calculations. Pressure interpolation is conducted with the PRESTO scheme, while pressure velocity coupling is accomplished by means of the SIMPLE algorithm. The pressure implicit with splitting of operators (PISO) is part of the SIMPLE family of algorithms is used for pressure–velocity coupling scheme. The PISO algorithm in comparison with the SIMPLE and SIMPLEC algorithms carries out two additional corrections including neighbor correction and skewness correction. The efficiency of calculations is improved by these correlations. The second-order upwind of discritization scheme is used in momentum, energy, and the two turbulent equations. A good convergence of simulation test is obtained if the under-relaxation factors be adopted at values of 0.8 (pressure), 0.3 (density), 0.3 (body force), 0.3 (momentum), 0.5 (turbulent kinetic energy), 0.5 (turbulent dissipation rate), 0.5 (turbulent viscosity), and 0.5 (energy). The mathematical formulation of VOF model is represented as follows.

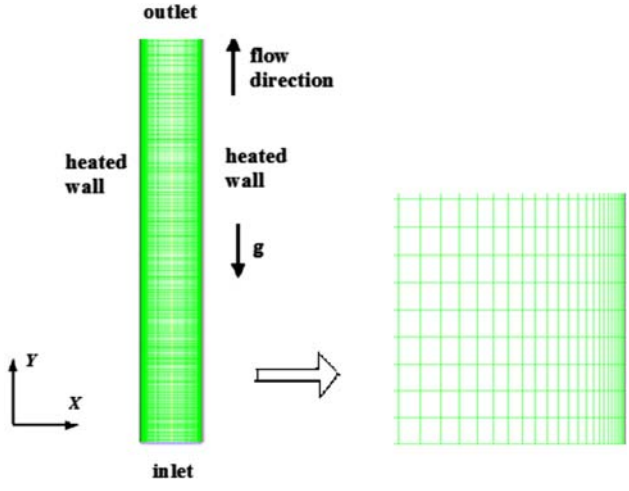

Fig 1. Schematic diagram of vertical duct.

4. VOF method

The VOF method can model two or more immiscible fluids by solving a single set of momentum equations and tracking the volume fraction of each of the fluids throughout the domain. In this method, a surface tracking technique is applied to each computational cell where the position of the interface between the fluids is of interest. The VOF formulation relies on the fact that two phases are not interpenetrating.

In VOF model, the summation of volume fractions of all phases is unity. The volume fraction equation will not be solved for the primary phase; the primary-phase volume fraction in a computational cell can be calculated according to the following constraint.

$$\alpha_f + \alpha_g = 1 \tag{1}$$

In which α_f and α_g denote the volume fraction of the liquid phase and vapor phase, respectively. Information of the phase distribution can be directly obtained from the volume fractions. As an instance, the computational grid is empty $\alpha_f = 0$ or full of liquid $\alpha_f = 1$, and $0 < \alpha_f < 1$. The continuity equation for the volume fraction of the phases has the following form:

$$\frac{\partial \alpha_f}{\partial t} + \vec{\nabla} \cdot (\vec{u}\alpha_f) = \frac{-S}{\rho_f} \tag{2}$$

$$\frac{\partial \alpha_g}{\partial t} + \vec{\nabla} \cdot (\vec{u}\alpha_g) = \frac{S}{\rho_g} \tag{3}$$

In which, the mass source term of S, kg/(m^3 s) on the right-hand side of continuity Eqs. (2) and (3) is specified a user-defined mass source term for each phase due to phase change.

The usual Navier–Stokes equations are solved for momentum in the cells, where only one of the two phases exists. At the interface, the force due to the surface tension must be taken into account. The momentum equation depends on the volume fractions of all phases through the properties ρ and μ.

$$\frac{\partial}{\partial t}(\rho \vec{v}) + \nabla.(\rho \vec{v}\vec{v}) = -\nabla p + \nabla \cdot [\mu(\nabla \vec{v} + \nabla \vec{v}^T)] + \rho \vec{g} + \vec{F}_\sigma \tag{4}$$

In which $\vec{F}_\sigma$ is the volumetric surface tension force.

Also, the energy equation shared among the phases is represented as:

$$\frac{\partial}{\partial t}(\rho E) + \nabla \cdot [\vec{u}(\rho E + p)] = \nabla \cdot (k_{eff} \nabla T) + Q \tag{5}$$

$$E = (\alpha_f \rho_f E_f + \alpha_g \rho_g E_g)/(\alpha_f \rho_f + \alpha_g \rho_g) \tag{6}$$

where E_f and E_g are defined based on the specific heat of liquid and vapor phases and the shared temperature is represented as:

$$E_f = C_{g,f}(T - 298.15), \quad E_g = C_{g,g}\,(T - 298.15) \tag{7}$$

The source term Q (W/m^3), includes the heat transfer rates through the interface, in Eq. (5). The properties ρ and k_{eff} (effective thermal conductivity) are shared by the phases.

$$\rho = \alpha_f \rho_f + \alpha_g \rho_g \tag{8}$$

$$\mu = \alpha_f \mu_f + \alpha_g \mu_g \tag{9}$$

$$k_{eff} = \alpha_f k_{eff,f} + \alpha_g k_{eff,g} \tag{10}$$

In the VOF model, the accuracy of the temperature near the interface is limited in cases, where large temperature differences exist between the phases.

The surface tension force is calculated for the cells containing the vapor–liquid interface [8]. The surface tension can be written in terms of the pressure jump across the surface set as the source term, which is added to the momentum equation and has the following form:

$$F_\sigma = \sigma \frac{\alpha_f \rho_f k_g \nabla \alpha_g + \alpha_g \rho_g k_f \nabla \alpha_f}{0.5(\rho_f + \rho_g)} \tag{11}$$

In which σ is the interfacial tension force between the phases, and the curvatures of the phases set as;

$$k_f = \frac{\nabla \alpha_f}{|\nabla \alpha_f|}, \quad k_g = \frac{\nabla \alpha_g}{|\nabla \alpha_g|} \tag{12}$$

5. Phase change modeling

5.1. Mass source term

A mass transfer model including of evaporation process is adopted to simulate mass transferring from liquid to vapor phase [9]. The mass source term, mostly depends on the saturation temperature. If $T \geq T_{sat}$, the saturation occurs. The mass transfer rate of the liquid and vapor phases in the control volume decreases and increases, respectively, which means that the mass transfer direction is from the liquid phase to the vapor phase. The magnitude of mass transfer rate is represented in the following form.

$$S = c_f \alpha_f \rho_f \frac{T - T_{sat}}{T_{sat}} \tag{13}$$

If $T < T_{sat}$, the condensation occurs. The mass transfer rate of the liquid and vapor phase in the control volume increases and decreases, respectively, which means that the mass transfer direction is from the vapor phase to the liquid phase. The magnitude of mass transfer rate is as the follows;

$$S = c_g \alpha_g \rho_g \frac{T - T_{sat}}{T_{sat}} \quad (14)$$

In which, c_f and c_g are the empirical coefficients in range of 0.1–100 s^{-1} in order to numerically maintain the interface temperature at T_{sat}, and the choice was justified by a good agreement between the model prediction and the experiment. Exclusively, large values of c_f and c_g lead to a numerical convergence problem, whereas the small ones cause a significant deviation between the interfacial and saturation temperatures [10].

5.2. Heat source term

The heat transfer can be obtained if the mass source term be considered as follows:

$$Q = S \cdot h_{fg} \quad (15)$$

In which h_{fg} is the latent heat.

Finally, VOF equation, continuity, momentum, and energy equation should be solved with each other to obtain pressure, velocity, and temperature magnitude in each cell.

6. Results and discussion

In this study, water is used as the working fluid and the value of the interfacial tension force, σ, is adopted by the temperature. The values of physical properties of water are specified by inlet temperature and system pressure. Also, the gravity acceleration, g, is considered to be 9.81 m/s^2.

The heat transfer and the wall temperature of a uniform heated tube at two different conditions have been analyzed numerically by an unsteady solution in two different times. The diameter and height of the tube are 33.3 mm and 500 mm, respectively. Table 1 demonstrates conditions used in numerical analyses in which $\dot{m}$, T_i and T_{wall} denote mass flow rate, inlet temperature, and wall temperature, respectively.

The temperature of the liquid along the length of tube increases as it is heated, and the saturation point temperature of the liquid falls due to the decrease in hydrostatic pressure along the length of tube. While the liquid temperature increases, the difference $T_{wall} - T_{liquid}$ gets lower until the saturation condition is reached. Fig. 2 shows the contours of volume fraction (vapor) in subcooled flow boiling and saturated flow boiling regions in two conditions (I and II). The height of subcooled flow boiling region in condition I is higher than that in condition II. The main mechanism of flow boiling is the latent heat of evaporation on the heated surface [7]. This mechanism gets more prominent at high pressures compared to the normal pressure [11]. When the bubbles are still attached to the heated surface, the heat is transported by evaporation mechanism at the root of the bubbles; then, the bubble agitation of thermal boundary layer adjacent to the heated surface causes the fluctuations of volume fraction on the heated wall. Small bubbles attached to the heated wall were observed in subcooled flow boiling region. In upstream of the region, since the void fractions are low and the bubbles are static in size, the condensation heat flux from the top of the bubbles is balanced to the boiling heat flux. In downstream of the region, the heating wall is covered by several layers of bubbles with whole energy from the wall utilized for vapor generation. Fig. 3 shows the distribution of volume fraction (vapor) in conditions I and II for the tube wall and tube axis. Fig. 3(a) depicts the fluctuations of volume fraction on the heated wall due to bubble agitation of the thermal boundary layer in conditions I and II. The subcooled flow boiling zone of the tube length in conditions I and II are $0 < x < 0.05$ and $0 < x < 0.025$, respectively. As it can be seen in Fig. 3(b), there is no variation of void fraction on the tube center in subcooled flow boiling region; but in saturated flow boiling region, the volume fraction increases in the center of tube length. The fluctuations of the vapor volume fraction are due to the phase change mechanism and variations in thermophysic properties of liquid–vapor phases such as thermal conductivity on the heated wall.

It is obvious that for control volumes which exist on liquid–vapor interface, the value of temperature is equal to saturated temperature of the liquid. Therefore, for control volumes including the interface, the temperature is the same as the saturation temperature.

Table 1
Values of properties used in the numerical analysis

Conditions	Motive steam pressure (bar)	$\dot{m}(kg/s)$	T_i (K)	T_{wall} (K)
Condition I	99.7	0.0477	583	613
Condition II	10.5	0.0477	450	480

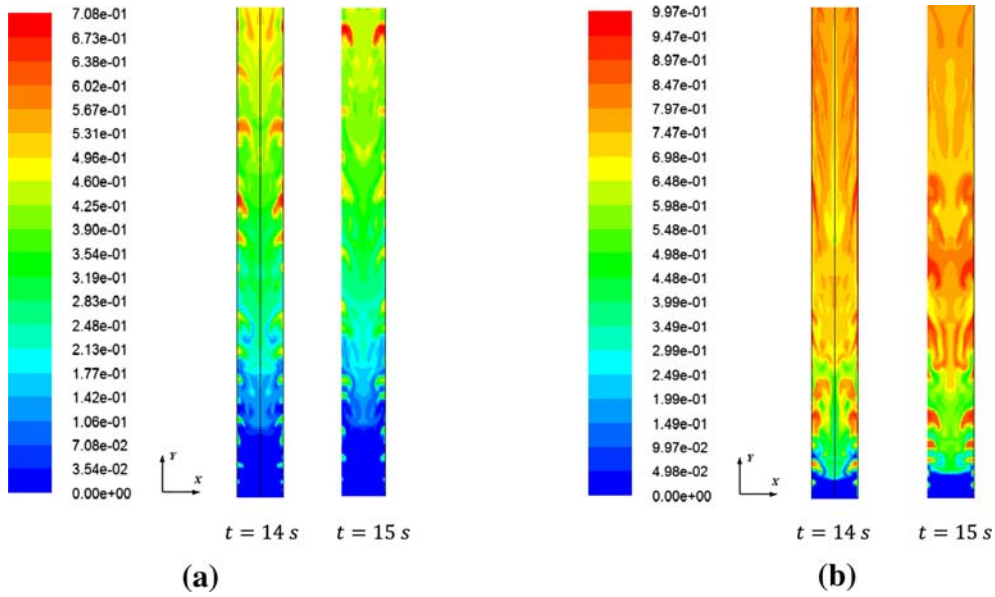

Fig 2. (a) Contours of volume fraction (vapor) in condition I. (b) Contours of volume fraction (vapor) in condition II.

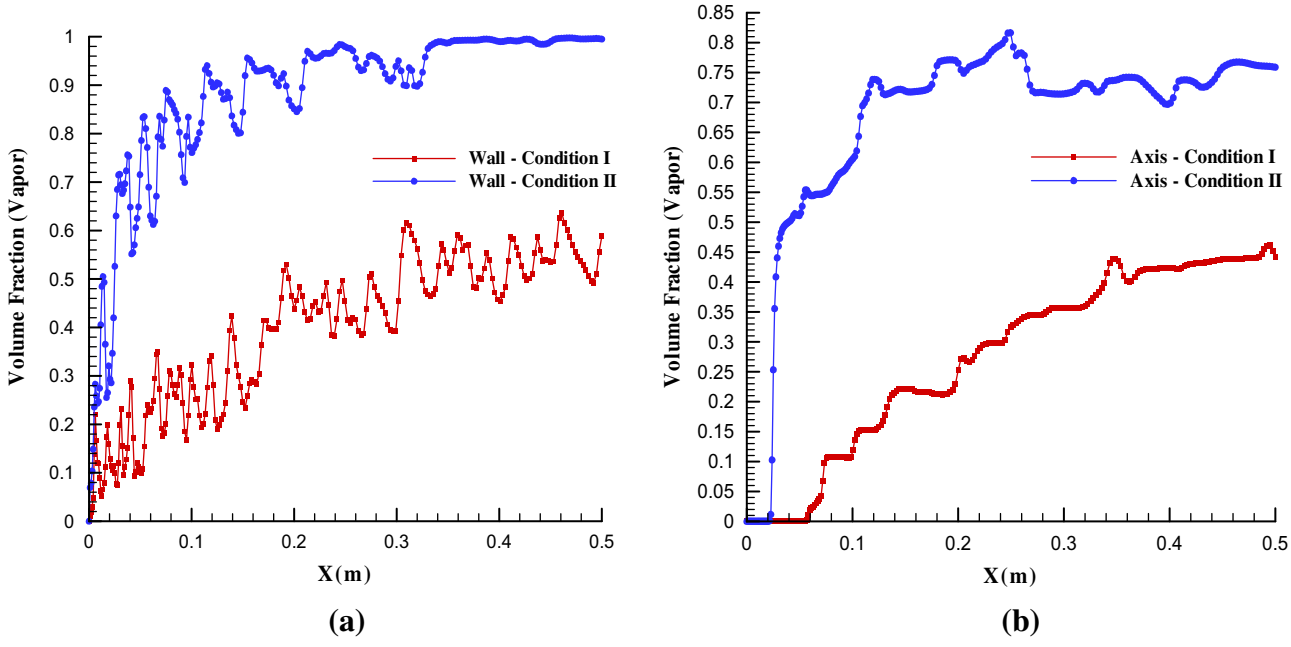

Fig. 3. Distribution of volume fraction (vapor) in condition I & condition II: (a) tube wall and (b) tube axis.

Fig. 4 shows the heat transfer coefficient of fluid on the heated wall along the tube length. It can be observed that the behavior of the heat transfer coefficient is similar to the vapor volume fraction on the wall, since the heat transfer coefficient of fluid is decreased due to the increase in vapor volume fraction. Also, the fluctuations found on vapor volume fraction are transmitted to the heat transfer coefficient. Moreover, the jumping of heat transfer coefficient is due to nucleation boiling and phase change mechanism of liquid–vapor phases on the heated wall. In addition, the amount of heat transfer coefficient strongly depends on the boundary layer thickness. Vapor velocity and temperature difference between

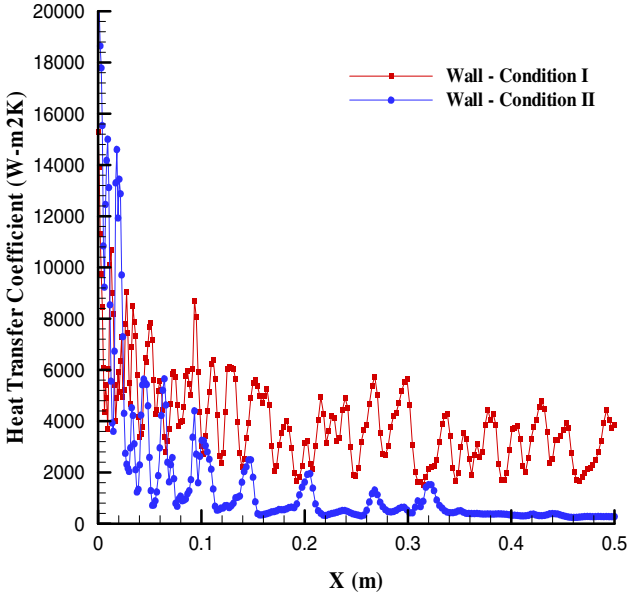

Fig. 4. Distribution of heat transfer coefficient in condition I and condition II.

the wall and saturation temperature are affected by boundary layer thickness.

Distribution of the wall temperature is represented in Fig. 5 as a function of the tube length. As it can be seen, the fluctuation of wall temperature in condition I is more than that of condition II. The sudden decrements of the wall temperature are due to the jump in the increased value of the convection heat transfer coefficient in conditions I and II.

7. Comparison with experimental data

To verify numerical simulation of evaporation heat transfer coefficient, numerical results were compared with experimental results of film boiling heat transfer of water flowing upwards in a duct accomplished by Johannsen et al. [12]. They used a vertical tube in which water moves under effect of the gravity. In Fig. 6(a), the average heat transfer coefficient corresponding to the numerical simulation approach is compared with experimental data. The jump of the heat transfer coefficient on the surface is due to the variation of thermophysic properties such as thermal conductivity of liquid–vapor phases formed on the heated wall, and the increase in the vapor phase velocity compared to the liquid phase. Also, the velocity vectors of stream function in the numerical modeling are shown in Fig. 6 (b). It can be seen that vortexes formed on the heated surface is caused by velocity of the vapor phase due to phase change and dynamic instability of vorticity. Moreover, in the case of turbulent evaporation flow, the surface tension between the phases and vapor velocity on the heated wall can be created vortex flow near the wall. Then, the vapor velocity vectors near the wall are increased as a result of liquid–vapor interface on the control volume due to the evaporation.

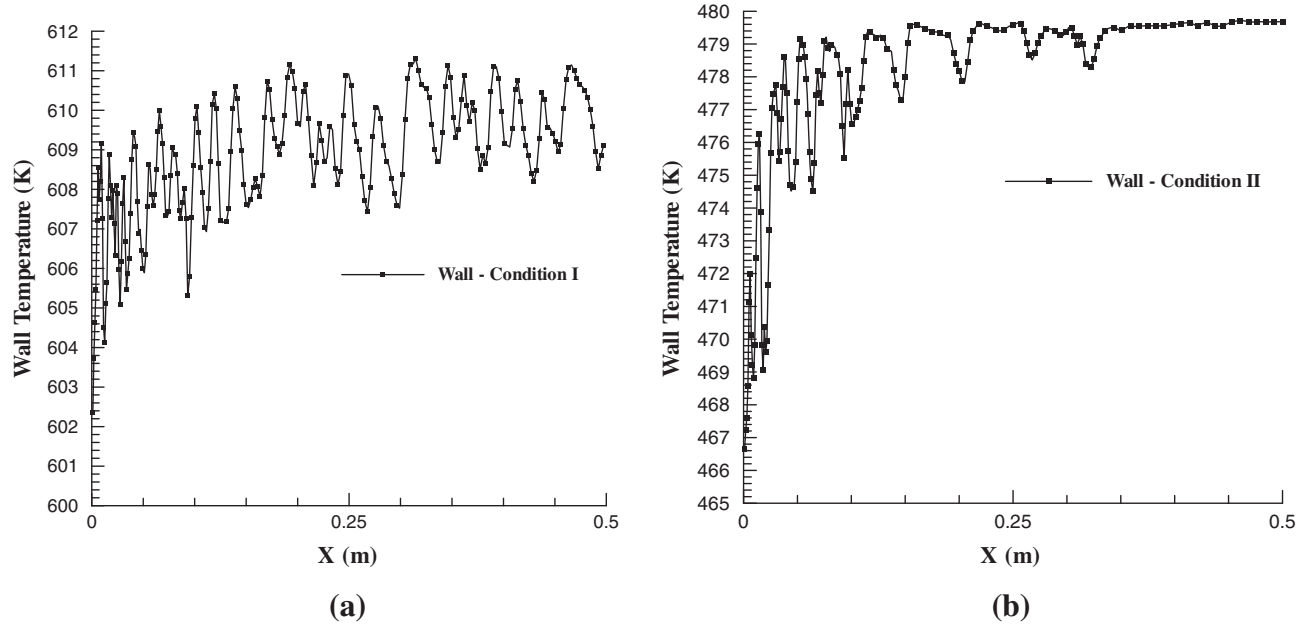

Fig 5. (a) Distribution of wall temperature in condition I. (b) Distribution of wall temperature in condition II.

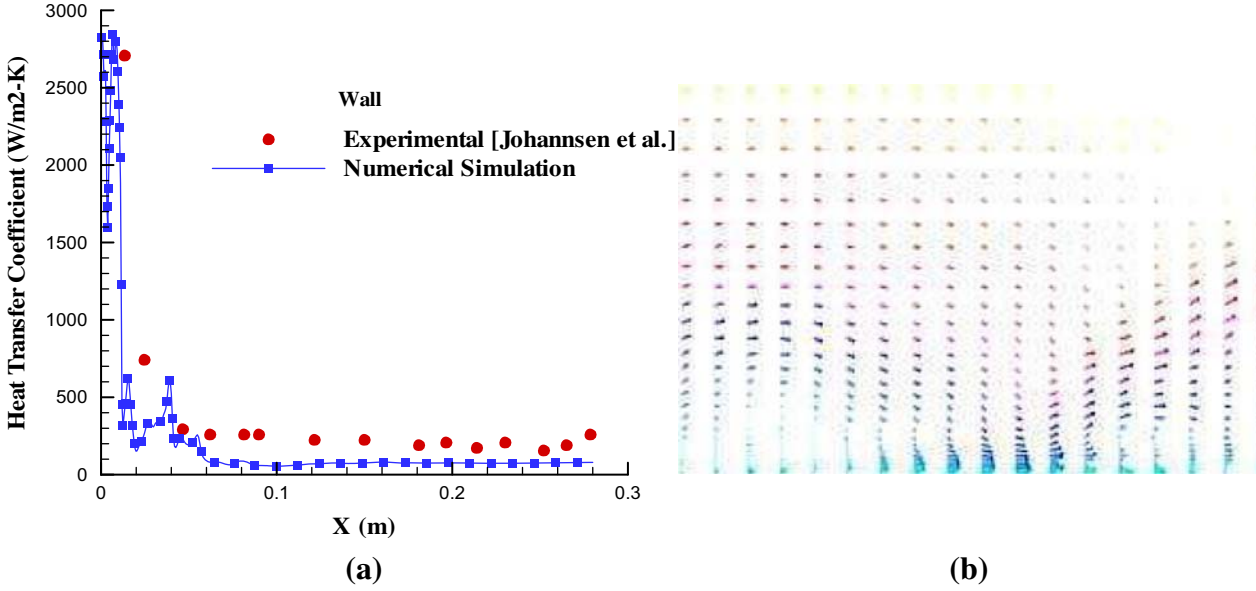

Fig 6. (a) Comparison of numerical simulation with experimental data. (b) Velocity vectors of stream function on the wall tube.

8. Conclusions

In this study, a numerical simulation of transient solution of two-phase flow was accomplished in an upward vertical tube. The phase change modeling for the heat transfer mechanism is energy and mass transfer using the VOF model in conjunction with the UDF as evaporation. The effect of volume fraction on the heat transfer coefficient was investigated along the tube length. In order to improve the efficiency of calculations, the PISO algorithm was employed. The average of surface heat transfer coefficient obtained from the present numerical simulation profile was compared with that of experimental result and a good agreement was found. The main conclusions can be summarized as follows:

- The fluctuations of volume fraction are owing to the bubble agitation of thermal boundary layer adjacent to the heated wall, and thermophysic properties variations of liquid–vapor phases such as thermal conductivity due to the phase change mechanism. Furthermore, due to the oscillations of liquid–vapor interface on the surface, fluctuations of vapor volume fraction in high pressure (condition I) are more than those in low pressure (condition II). Also, the behavior of fluctuations found in vapor volume fraction is transmitted to the heat transfer coefficient and wall temperature due to control volumes including the liquid–vapor interface on the heated wall.
- The distance of subcooled flow boiling region between the onset of nucleation boiling point and the saturation point in high pressure (condition I) is higher than that of low pressure (condition II).
- The amounts of formed vapor volume fraction in low pressure condition are higher than those of high pressure condition.
- The amounts of average heat transfer coefficient on the wall in high pressure are more than those in low pressure. The surface heat transfer coefficient gets lower, when the vapor volume fraction is increased. So, the behavior of the surface heat transfer coefficient along the tube length is similar to the surface heat flux.

References

[1] R. Kouhikamali, A. Samami, M. Asgari, F. Alamolhoda, The effect of condensation and evaporation pressure drop on specific heat transfer surface area and energy consumption in MED-TVC plants, Desalin. Water Treat. 46 (2012) 68–74.
[2] D. Steiner, J. Taborek, Flow boiling heat transfer vertical tubes correlated by an asymptotic model, Int. J. Heat Transfer Eng. 13 (1992) 43–69.
[3] J. R. Thome, Boiling of new refrigerants: a state-of-the-art review, Int. J. Refrig. 19 (1996) 435–457.
[4] S. G. Kandlikar, Development of flow boiling map for subcooled and saturated flow boiling of different fluids inside circular tubes, Int. J. Heat Transfer 113 (1991) 190–200.
[5] W.H. McAdams, W.E. Kennel, C.S. Minden, P.M. Picornell, J. E. Dew, Heat transfer at high rates to water with surface boiling, Ind. Eng. Chem. 41 (1949) 1945–1945.
[6] V. Prodanovic, D. Fraser, M. Salcudean, On the transition from partial to fully developed boiling subcooled flow boiling, Int. J. Heat Mass Transfer 45 (2002) 4727–4738.

[7] R. Kouhikamali, Numerical simulation and parametric study of forced convective condensation in cylindrical vertical channels in multiple effect desalination systems, Desalination 254 (2010) 49–57.
[8] J.U. Brackbill, D B. Kothe, C.A. Zemach, Continuum method for modeling surface tension, J. Computat. Phys. 100 (1992) 335.
[9] Jing-hua Wei., Liang-ming Pan, De-qi Chen, Hui Zhang, Xu Jian-jun, Yan-ping Huang, Numerical simulation of bubble behaviors in subcooled flow boiling under swing motion, Nuclear Eng. Des. 241 (2011) 2898–2908.
[10] Z. Yang, X. F. Peng, P. Ye, Numerical and experimental investigation of two phase flow during boiling in a coiled tube, Int. J. Heat Mass Transf. 51 (2008) 1003–1016.
[11] M. Jamialahmadi, R. Blochl, H. Muller-Steigen, Bubble dynamics and scale formation during boiling of aqueous calcium sulfate solution, Chem. Eng. Process 26 (1989) 15–26.
[12] M. Mosaad, K. Johannsen, Experimental Study of Steady-State Film Boiling Heat Transfer of Subcooled Water Flowing Upwards in a Vertical Tube", Exp. Thermal Fluid Sci. 2 (1989) 477–485.